Vol. **112** (2007) *ACTA PHYSICA POLONICA A* Supplement

Proton Transfer in Strong Hydrogen Bonds Revealed by Infrared Spectra — Correlations between Structure and Spectra for the BrH : NH_3 Complex

K. Szczepaniak and W.B. Person

Department of Chemistry, University of Florida
P.O. Box 117200, Gainesville, Florida, 32611, USA

Dedicated to the memory of our good friend Jerzy Prochorow

One of our most pleasant memories is of the afternoon during our last visit in Poland spent walking and talking with Jerzy and Halina P. in Wilanów Park. One topic of that conversation concerned the possibility of sending him a manuscript for possible publication in *Acta Physica Polonica A*. It has been a disappointingly slow process, but we humbly and belatedly offer this to honor his memory.

Our scope is to achieve an understanding of the relation between the infrared spectrum and structure of a strong hydrogen-bonded complex, BrH : NH_3, and how and why this relationship is affected by the environment surrounding the complex. A series of DFT/B3LYP/6-31G(d,p) calculations was carried out for this system to obtain its structure and spectrum in different dielectric fields characterized by their relative permittivities. Changes in structure and spectrum (both frequencies and intensities) as the relative permittivity changes are explored. Calculations of spectra are made first under the harmonic approximation. In the next step the effect of anharmonicity was estimated for several different dielectric fields. The calculated anharmonic spectrum (for $\varepsilon_r = 1.6$) is compared with the experimentally observed infrared spectrum of the complex isolated in an Ar matrix at 10 K, obtained in our laboratory. The calculated frequencies and relative intensities for all normal modes agree with the corresponding experimental data surprisingly well. The potential usefulness of structure-spectra correlations is explored.

PACS numbers: 82.30.Rs, 33.20.Ea, 33.70.Fd, 31.15.Ew, 33.20.Tp

1. Introduction

Hydrogen bonds between proton donors and proton acceptors play an essential role in determining the properties of molecular systems, including those in living organisms. The infrared spectrum is very sensitive to the position of the proton and may provide quantitative information about the geometry of the complex, when combined with quantum mechanical calculations. Use of matrix isolation in noble gas solids offers a unique opportunity to study spectra over the entire mid-infrared region (no interfering absorption from the solvent) which is often of crucial importance for strongly hydrogen bonded complexes. In this paper we focus our attention on the hydrogen bond between the strong acid hydrogen bromide (HBr) and the base ammonia (NH_3), abbreviated in the following text by $BrH_b : NH_3$ (the "b" subscript designates the atom involved in the hydrogen bond). It is one of the simplest examples of a strong hydrogen bond in which proton transfer from BrH_b to NH_3 is promoted by the environment. Although we are focusing on this particular system, we believe that the results presented below will be useful in understanding properties — particularly infrared spectra including intensities — of hydrogen bonded complexes in general.

Any interaction of the hydrogen bonded complex with its surrounding may cause changes in the structure and spectra of the complex from those found in the gas phase (see recent papers and references therein [1–5]). In this work we consider changes in the hydrogen bonded complex that are caused by the reaction field in a dielectric medium. Recent studies (e.g. [1–5]) indicate that this effect is very dramatic.

We carried out quantum-mechanical calculations of structure and infrared spectra of the $BrH_b : NH_3$ complex over a range of dielectric fields of varying strength characterized by the relative permittivity (dielectric constant) ε_r. These calculations provide data on changes of geometry and spectra (frequencies and intensities) as well as the description of the normal modes and allow examination of trends in the correlations between the structural and spectroscopic parameters. The results are very helpful in the interpretation of experimental spectra (particularly the observed intensity patterns) of the $BrH_b : NH_3$ complex isolated in low temperature matrices formed of solid noble gases or of solid N_2, including studies from our laboratory.

The studies reported here are an extension of earlier attempts to combine results from quantum-mechanical calculations with experimental study of vibrational spectra of matrix-isolated molecules and complexes (for example see [6–10]). In this paper we carry out density functional theory (DFT) calculations (see references 19–21 in [8]), which are capable of providing good values for vibrational frequencies and intensities at a considerably lower computational cost and our time than for post-HF methods as used in [6] and [7].

2. Quantum-mechanical calculations of the effect of dielectric field on the properties of BrH_b:NH_3

The effect on the structure and infrared spectra that occurs for hydrogen bonded complexes in a dielectric medium is evaluated using the Onsager model for the field effect with Gaussian program G98W [11]. The calculations were carried out on a Personal Computer (Dell 8300 under Windows XP Professional) at the DFT B3LYP/6-31G(d,p) level of theory. The details and references for these DFT calculations were described in [8], as were those concerning the analysis of the calculated data by other programs developed for use in our laboratory (ANIMOL for visualizing the normal coordinate displacements, XTRAPACK for calculating potential energy distributions and intensity distributions, and Anharmonic program in $\text{MathCad}^{\text{tr}}$ to calculate the correction for anharmonicity). In this paper we shall not repeat these previous descriptions.

2.1. Effect of dielectric field on structure

The hydrogen bond in $BrH_b : NH_3$ is linear, imposing constraints on the distances ($R(BrH_b) + R(H_bN) = R(NBr)$) and the angle ($A(BrH_bN) = 180°$). The C_{3v} symmetry of the complex imposes further constraints, so that the structure is described by values of 6 independent coordinates; namely $R(BrH_b)$, $R(H_bN)$, $R(NH_i)$, $A(BrH_bN)$, $A(H_bNH_i)$ and $A(H_iNH_j)$ (i and j relate to the hydrogen atoms of the NH_3 fragment).

Values for the equilibrium distances most sensitive to the change of the environment ($R(BrH_b)$, $R(H_bN)$, $R(NBr)$) are shown in Table I. These results are from calculations B3LYP/6-31G(d,p) using self-consistent reaction field (SCRF) model (key words: SCRF = DIPOLE; OPT = Tight; at a calculated cavity radius of 3.21 Å [11]). The values of the relative permittivity ε_r in the table are from 1.00 to 7.00, covering the range from gas phase to solid NH_4Br.

Each row in Table I lists properties of the equilibrium structure found in the SCRF calculation for the complex in the field with relative permittivity ε_r. As can be seen in the table, the values for the properties are quite sensitive to ε_r, particularly in the range from 1.0 to 2.0, where major structural changes are found for small changes of ε_r. For ε_r greater than 2.0, the changes in structure are much more gradual so that wider intervals for ε_r are sufficient to show trends there.

It is instructive to present some of the results listed in Table I in terms of correlation diagrams showing the trends in changing of the properties with the relative permittivity of the environment. Figure 1 shows the correlation of $R(BrH_b)$ and $R(NH_b)$ with ε_r (from 1.00 to 7.00). Figure 2 shows a similar correlation diagram for the $R(BrN)$.

The abrupt change of $R(BrH_b)$ and $R(NH_b)$ distances in Fig. 1 and of $R(NBr)$ in Fig. 2 identifies the proton transfer reaction occurring for ε_r between 1.472 and 1.475, marking a transition region from the neutral-molecule structure

TABLE I

Calculated equilibrium distances (in [Å]) R_e(BrH), R_e(NH) and R_e(NBr) of BrH_b:NH_3 complex in different dielectric field characterized by relative permittivity ε_r.

ε_r	R_e(HBr)	R_e(NH)	R_e(NBr)
1.000	1.5108	1.6516	3.1624[a]
1.100	1.5199	1.6243	3.1442
1.200	1.5307	1.5957	3.1264
1.240	1.5352	1.5838	3.1190
1.300	1.5438	1.5642	3.1080
1.350	1.5511	1.5451	3.0970
1.400	1.5609	1.5246	3.0855
1.450	1.5759	1.4935	3.0694
1.460	1.5812	1.4843	3.0655
1.465	1.5847	1.4782	3.0629
1.470	1.5879	1.4722	3.0600
1.472	1.5897	1.4689	3.0586
1.475	1.6564	1.3664	3.0228
1.480	1.6648	1.3551	3.0198
1.500	1.6832	1.3310	3.0142
1.520	1.6957	1.3156	3.0113
1.550	1.7110	1.2978	3.0088
1.600	1.7322	1.2750	3.0072
1.630	1.7436	1.2637	3.0073
1.650	1.7507	1.2570	3.0076
1.700	1.7671	1.2422	3.0093
1.800	1.7946	1.2202	3.0148
1.900	1.8154	1.2046	3.0200
2.000	1.8316	1.1936	3.0252
2.200	1.8575	1.1774	3.0349
2.500	1.8870	1.1611	3.0480
3.000	1.9259	1.1429	3.0688
5.000	2.0536	1.1040	3.1576
7.000	2.1584	1.0854	3.2438

[a]Experimental R(NBr) = 3.255 Å, Ref. A.C. Legon, *Chem. Soc. Rev.* **22**, 153 (1993).

(BrH_b : NH_3) to the ion–pair structure (Br^-:$H_bNH_3^+$) (the ammonium ion bonds through one of its N–H bonds to a bromide ion, with C_{3v} symmetry).

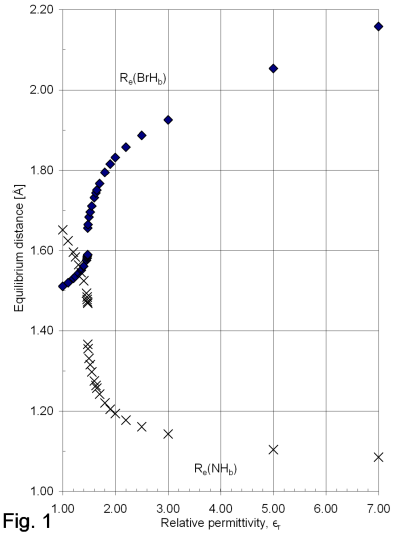

Fig. 1

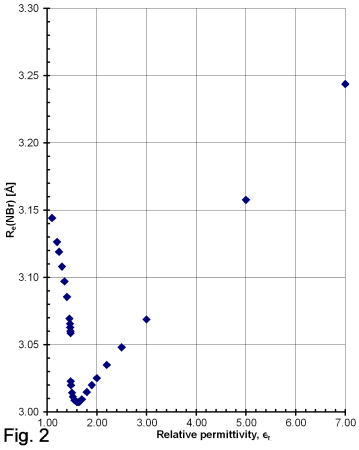

Fig. 2

Fig. 1. Correlation of the calculated equilibrium distances R_e(BrH) — filled diamonds and R_e(NH) — crosses with ε_r, for BrH:NH_3.

Fig. 2. Correlation of the calculated equilibrium distance R_e(NBr) of the BrH:NH_3 complex with ε_r.

2.2. Effect of dielectric field on infrared spectra

The DFT calculations described in the previous section using the Onsager model to obtain the optimized geometry for the BrH_b : NH_3 complex were extended to carry out calculations of the frequencies and intensities for the eight (4 in the a_1 symmetry class and 4 doubly degenerate modes in the e class) normal modes that define the infrared spectrum of the complex in the different environments characterized by ε_r. Because of the C_{3v} symmetry, the internal coordinates of a_1 symmetry do not interact with those of e symmetry.

The calculation is made assuming first that the potential energy is harmonic. The possible effects due to anharmonicity will be discussed in Sect. 2.3.

The names of the normal modes for the complex vary by author, but the usual practice is to use names that describe the predominant internal symmetry coordinate for each vibration of the isolated complex. We shall use the following names or abbreviations given below in parentheses for the four a_1 modes: $\nu 1$ — NH_3 symmetric stretch (NH_3 s str); $\nu 2$ — hydrogen bonded proton stretch (P str); $\nu 3$ — NH_3 umbrella bend (NH_3 umb); and $\nu 4$ — dimer stretch (Di str). For the four doubly degenerate e normal modes: $\nu 5$ — NH_3 asymmetric stretch (NH_3 as str); $\nu 6$ — NH_3 asymmetric deformation (NH_3 as def); $\nu 7$ — BrH_bN bend; and $\nu 8$ — NH_3 rock.

2.2.1. Normal modes of a_1 symmetry

Table II lists the frequencies of the a_1 normal modes ($\nu 1$, $\nu 2$, $\nu 3$, and $\nu 4$) of the $BrH_b : NH_3$ complex in different dielectric fields. Each row in Table II lists values for all 4 normal modes from the SCRF calculation for the Onsager dielectric field characterized by the value of ε_r given in the first column. The frequencies and intensities of each normal mode are listed in alternating columns across the table. For comparison the corresponding data for the vibrations of HBr, NH_3, and NH_4^+ monomers calculated at the same level of theory (for $\varepsilon_r = 1$) are listed in the footnotes of Table II. It should be noted that use of the word "intensity" or "intensities" in this paper is an abbreviation for the longer IUPAC-recommended term: "integrated absorption intensity A (against wave number) in units of km mol^{-1}" [12].

The effect of the dielectric field on the frequency and intensity of each normal mode of the complex can be seen by scrolling down the corresponding columns in Table II. This examination shows that the frequency of normal mode $\nu 1$ (NH_3 s str) does not change very much (by less than 1.5% for a change of ε_r from 1.0 to 7.0). The intensity changes from 5 to 110 km mol^{-1}.

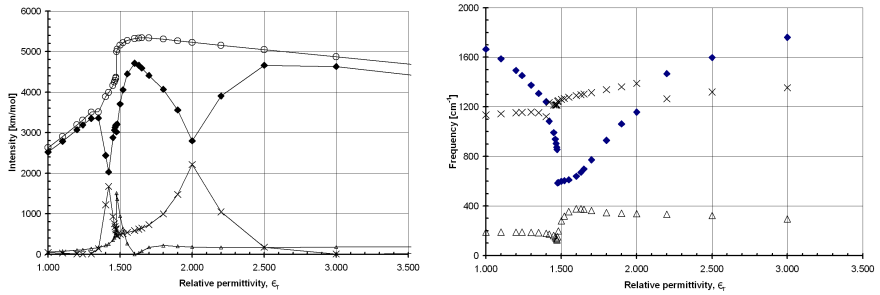

Fig. 3. Correlation with ε_r : right part — calculated frequencies of the normal modes $\nu 2$ — filled diamonds; $\nu 3$ — crosses; $\nu 4$ — triangles; left part — calculated intensities $A2$ — filled diamonds; $A3$ — crosses; $A4$ — triangles; total intensity ($A1+A2+A3+A4$) — circles.

The values for the other three a_1 normal modes are much more affected by the change of the field, as seen in Table II and Fig. 3. In Fig. 3 (right) correlation diagrams of the frequencies $\nu 2$, $\nu 3$, and $\nu 4$ with ε_r are shown. Figure 3 (left) presents the corresponding correlation for the intensities ($A2$, $A3$, and $A4$). (The diagram does not include $\nu 1$ because changes for it are quite small.)

There is a smooth decrease in the frequency of $\nu 2$ and increase in its intensity (with little change in frequency and intensity for $\nu 3$ or $\nu 4$) until ε_r is somewhere between 1.35 and 1.42, where the frequency of $\nu 2$ approaches that of $\nu 3$. For ε_r between 1.35 and 1.48 dramatic decreases of both frequency and intensity of $\nu 2$ occur, accompanied by a strong increase in intensity for the $\nu 3$ mode. These changes reflect the changing character of the normal modes; as seen in Fig. 4.

TABLE II

Calculated frequencies — νi — in [cm^{-1}] and intensities — Ai in [km/mol] of normal modes of a_1 symmetry of BrH_b:NH_3 complex in different dielectric field characterized by relative permittivity ε_r.

ε_r	NH_3 s str		H_b str		NH_3 umb		Di str		$\sum Ai$
	$\nu 2$	$A1$	$\nu 2$	$A2$	$\nu 3$	$A3$	$\nu 4$	$A4$	
1.000	3480[a]	5[a]	**1665**[b]	**2520**[b]	1135[c]	44[c]	188	63	2631
1.100	3480	6	**1588**	**2788**	1144	29	188	78	2901
1.200	3478	7	**1494**	**3074**	1153	9	188	100	3190
1.240	3478	7	**1453**	**3190**	1155	2	188	112	3311
1.300	3474	8	**1375**	**3352**	1157	12	186	138	3510
1.350	3477	9	**1308**	**3361**	1153	141	184	168	3511
1.400	3473	10	**1242**	**2439**	1122	1221	177	219	3889
1.420	3475	10	**1084**	**2031**	1235	1672	173	255	3989
1.450	3475	11	**992**	**2876**	1214	930	161	348	4165
1.460	3474	12	**939**	**3063**	1215	754	150	414	4243
1.465	3475	12	**905**	**3134**	1214	681	141	466	4292
1.470	3473	12	**873**	**3179**	1215	628	132	521	4340
1.472	3473	12	**855**	**3194**	1216	604	126	555	4366
1.475	3467	17	**585**	**3019**	1244	459	150	1505	5000
1.480	3466	17	**588**	**3211**	1249	468	199	1358	5054
1.500	3464	18	**599**	**3707**	1260	493	278	941	5159
1.520	3463	19	**604**	**4055**	1267	512	318	631	5217
1.550	3462	20	**610**	**4448**	1277	538	353	267	5272
1.600	3460	22	**640**	**4713**	1291	584	377	2	5321
1.630	3458	23	**671**	**4662**	1298	619	377	31	5334
1.650	3458	23	**697**	**4593**	1303	645	374	76	5338
1.700	3456	25	**772**	**4411**	1315	729	363	172	5337
1.800	3452	28	**929**	**4068**	1338	995	346	216	5307
1.900	3452	30	**1062**	**3559**	1361	1478	340	198	5265
2.000	3451	32	**1157**	**2797**	1389	2216	338	183	5229
2.200	3448	36	**1468**	**3902**	1264	1047	333	168	5154
2.500	3446	42	**1598**	**4664**	1320	174	322	167	5047
3.000	3443	51	**1761**	**4631**	1355	8	294	181	4872
5.000	3434	83	**2198**	**3832**	1414	54	201	189	4158
7.000	3428	110	**2454**	**3186**	1442	105	129	183	3584

[a]For NH_3 monomer calculated frequency (m.c.f.) — 3462 cm^{-1}, intensity (int.) — 1 km/mol; for NH_4^+ m.c.f. — 3495 cm^{-1}, int. — 593 km/mol. [b]For BrH m.c.f. — 2563 cm^{-1}, int. — 4 km/mol. [c]For NH_3 m.c.f. — 1090 cm^{-1}, int. — 145 km/mol; for NH_4^+ m.c.f. — 1496 cm^{-1}, int. — 543 km/mol.

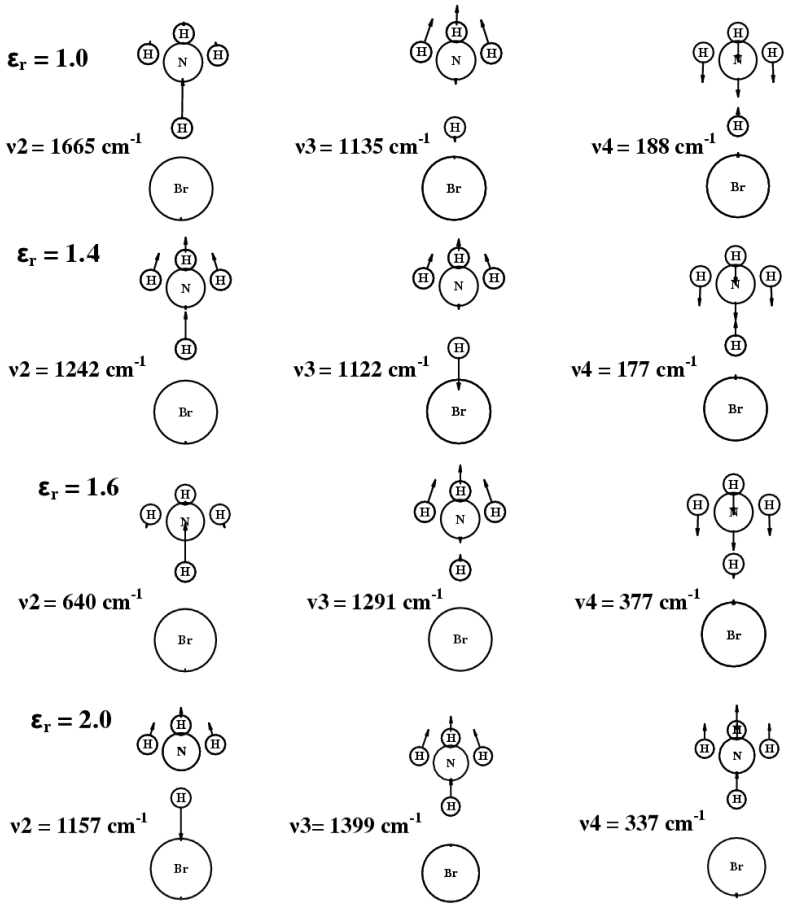

Fig. 4. Calculated displacement of atoms in normal modes $\nu 2$, $\nu 3$, and $\nu 4$ of the BrH:NH_3 complex in different dielectric fields characterized by ε_r. These displacements were drawn using the Animol program (see [8] for details) to analyze the data from Gaussian 98 output.

For $\varepsilon_r = 1.4$, $\nu 2$ and $\nu 3$ are no longer pure proton stretch and NH_3 umbrella bend, respectively, as they were for $\varepsilon_r = 1$ (shown also in Fig. 4). Instead, $\nu 2$ and $\nu 3$ both have large contributions from each of these two symmetry coordinates. An interaction between $\nu 2$ and $\nu 4$ (Di str) is apparent also for ε_r around 1.475, where a strong increase in the intensity of $\nu 4$ is observed. This interaction appears to be related to the "two-dimensional" coupling considered in [1]. The interaction involving $\nu 2$ and $\nu 4$ is complicated by the proton transfer reaction from the normal--molecule structure to the ion–pair structure that occurs for ε_r from 1.472 to 1.475, discussed in Sect. 2.1.

For ε_r greater than 1.6 the frequency of $\nu 2$ increases and its intensity decreases (reaching a minimum for $\varepsilon_r = 2.0$) shown in Fig. 3. In contrast, the

intensity of $\nu 3$ increases in this region of ε_r to a maximum at $\varepsilon_r = 2.0$ without very strong change in frequency. Again, these changes indicate that the interaction has changed the character of the normal modes.

This change of character of the mixing of the internal coordinates can be seen in Fig. 4 for $\varepsilon_r = 2.0$ and 1.6. As seen there, the character of $\nu 2$ is again pure proton stretch, and $\nu 3$ is pure NH_3 umbrella bend for $\varepsilon_r = 1.60$. Greater mixing of the symmetry coordinates for each normal mode occurs for $\varepsilon_r = 2.0$, rather similar to the mixing shown at $\varepsilon_r = 1.4$ (see Fig. 4). Let us note that the complex is in the ion–pair form for $\varepsilon_r > 1.60$.

As seen in Fig. 4, the character of $\nu 4$ (Di str) also changes for each value of ε_r, and has mixed contributions from the internal displacement coordinates for all.

It is worthwhile to note in Fig. 3 (left) that the total intensity of all four modes (marked by open circles) changes rather smoothly in this range of ε_r, in contrast with the ups and downs of the individual intensities ($A2$, $A3$, and $A4$).

2.2.2. Normal modes of e symmetry

Table III lists the frequencies of the e normal modes ($\nu 5$, $\nu 6$, $\nu 7$, and $\nu 8$) of the $BrH_b : NH_3$ complex in different dielectric fields. Each row in Table III lists values for all 4 normal modes from the SCRF calculation for the Onsager dielectric field characterized by the value of ε_r given in the first column. The frequencies and intensities of each normal mode are listed in alternating columns across the table.

It is clear from Table III that only the frequency $\nu 7$ of the perpendicular bending motion (BrH_bN bend) is sensitive to changes of ε_r, as illustrated in Fig. 5. Before the transition from the normal-molecule structure to the ion–pair structure, the frequency of this mode increases from a value of 889 cm^{-1} (at $\varepsilon_r = 1.0$) to 1089 cm^{-1} (at $\varepsilon_r = 1.472$). After transition to the ion–pair structure (ε_r changes from 1.472 to 1.475), the frequency of this motion increases from 1089 cm^{-1} to 1211 cm^{-1}, and then continues to increase smoothly with increasing value of ε_r to 1503 cm^{-1} at $\varepsilon_r = 7.0$.

The infrared intensities of the absorption by these degenerate normal modes are each much lower than the intensity of $\nu 2$ mode (P str) in Table II. The biggest intensity change occurs for the NH_3 as str $\nu 5$ (from 32 km mol^{-1} for $\varepsilon_r = 1.0$ to 302 km mol^{-1} for $\varepsilon_r = 7.0$). The total intensity of absorption by all class e normal modes shown in the last column of Table III ranges from only 210 km mol^{-1} (at $\varepsilon_r = 1.0$) to 558 km mol^{-1} (at $\varepsilon_r = 7.0$), compared with a range of 2631 to 5338 km mol^{-1} for the total intensity of all class a_1 modes, as shown in the last column of Table II.

The e modes are much less sensitive to the environment than are the a_1 modes and because there is no interaction of normal modes between the two symmetry classes, there is no enhancement of intensity of an e mode at the expense of the intensity of a nearby a_1 mode. The anharmonicity effect for e symmetry

TABLE III

Calculated frequencies — νi — in [cm^{-1}] and intensities — Ai — in [km/mol] of double degenerate e normal modes of BrH_b:NH_3 complex in different dielectric field characterized by relative permittivity ε_r.

ε_r	NH_3 as str		NH_3 as def		BrH_bN be		NH_3 rock		$\sum Ai$
	$\nu 5$	$A5$	$\nu 6$	$A6$	$\nu 7$	$A7$	$\nu 8$	$A8$	
1.000	3618[a]	32[a]	1674[b]	50[b]	889	88	261	39	211
1.100	3617	37	1674	52	916	89	270	38	216
1.200	3614	41	1674	55	946	89	278	37	222
1.240	3614	43	1674	55	959	89	280	36	223
1.300	3610	47	1673	57	981	89	290	35	228
1.350	3612	50	1672	58	1000	90	290	34	232
1.400	3608	54	1672	59	1024	89	299	33	236
1.420	3610	56	1671	60	1036	90	297	32	238
1.450	3611	61	1671	61	1059	89	300	31	241
1.460	3609	62	1671	61	1070	89	304	31	243
1.465	3610	64	1670	61	1078	89	304	31	244
1.466	3609	64	1670	61	1078	89	306	31	244
1.467	3609	64	1670	61	1080	89	306	31	244
1.468	3609	64	1670	61	1082	89	306	31	245
1.470	3609	65	1670	61	1085	89	307	30	245
1.472	3608	65	1670	61	1089	89	308	30	246
1.475	3603	89	1667	63	1211	89	324	24	265
1.480	3602	92	1667	63	1223	89	324	24	268
1.500	3600	99	1667	63	1250	91	324	21	275
1.520	3598	104	1666	63	1267	92	323	20	280
1.550	3596	110	1667	63	1287	94	323	19	287
1.600	3593	119	1667	63	1314	97	323	18	296
1.630	3591	124	1667	62	1327	99	324	17	301
1.650	3590	127	1668	62	1336	100	324	17	305
1.700	3588	133	1668	61	1354	103	325	16	313
1.800	3582	145	1670	58	1381	109	329	15	326
1.900	3580	154	1672	56	1399	114	328	14	338
2.000	3577	161	1673	55	1412	119	328	13	348
2.200	3573	174	1676	52	1429	128	328	12	365
2.500	3567	188	1680	48	1446	139	330	11	386
3.000	3559	208	1686	43	1465	154	333	10	415
5.000	3539	264	1704	28	1495	199	340	7	499
7.000	3525	302	1714	22	1503	228	340	6	558

[a]For NH_3 m.c.f. — 3591 cm^{-1}, int. — 1 km/mol. [b]For NH_3 m.c.f. — 1694 cm^{-1}, int. — 27 km/mol.

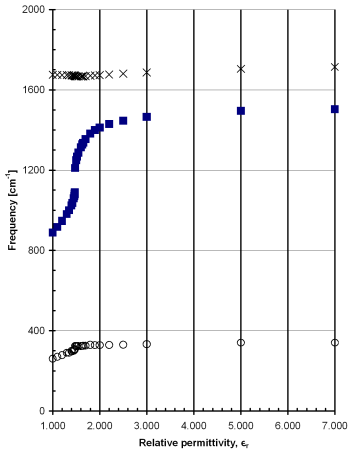

Fig. 5. Correlation with ε_r: calculated frequencies of the normal modes of e symmetry $\nu 6$ — crosses; $\nu 7$ — filled squares; and $\nu 8$ — circles.

modes is also expected to be much smaller than that for the a_1 mode $\nu 2$ discussed in Sect. 2.3.

2.3. Effect of anharmonicity

Results from calculations described above of the frequencies and intensities are subject to systematic errors, including the harmonic approximation. Hence, both calculated frequencies and intensities are expected to differ in value from those observed experimentally.

The most important effect of anharmonicity arises from the change in shape of the potential energy surface. The cross-section ("path") of the multidimensional energy surface followed by the H_b stretching coordinate is called the potential energy curve for the internal coordinate in the following text. These potential energy curves are computed at the DFT B3LYP\6-31G(d,p) SCRF level using the partial optimization method described in [13]. In this point-by-point calculation a constrained-geometry optimization (so-called relaxed scan) is performed at each value of the $R(BrH_b)$ distance to obtain the energy and geometry for the complex at the stationary point for this distance.

Figure 6 shows the relaxed energy curves of the complex obtained in this manner as a function of $R(BrH_b)$ for several ε_r values. The upper curve (marked by triangular points) in Fig. 6 shows this potential for the complex at $\varepsilon_r = 1.0$ (in vacuum). The other curves show how this potential changes in dielectric fields corresponding to $\varepsilon_r = 1.24$, 1.47, 1.6, 2.2, and 3.0.

As seen in Fig. 6, the equilibrium structure in vacuum is the neutral molecule complex ($Br–H_b:NH_3$) with $R(BrH_b) = 1.511$ Å. A vague shoulder appearing above the minimum (on the right side) hints at the contribution of the ion–pair structure ($Br^-:H_bNH_3^+$). At $\varepsilon_r = 1.24$ (close to that of solid Ne) the equilibrium

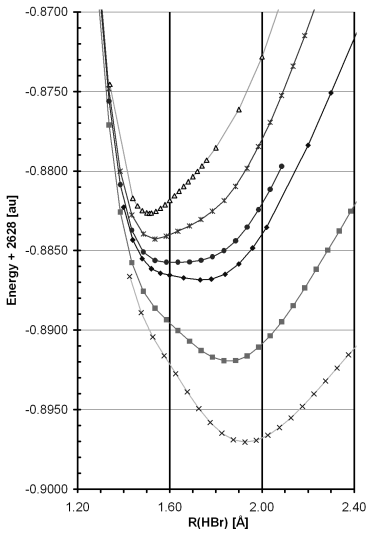

Fig. 6. Calculated relaxed energy curves as a function of BrH distance of the BrH : NH_3 complex in dielectric field characterized by ε_r — for $\varepsilon_r = 1.00$ — triangles; $\varepsilon_r = 1.24$ — stars; $\varepsilon_r = 1.47$ — filled circles; $\varepsilon_r = 1.60$ — filled diamonds; $\varepsilon_r = 2.20$ — filled squares; $\varepsilon_r = 3.00$ — crosses.

structure with $R(\mathrm{BrH_b}) = 1.535$ Å is still the neutral molecule complex but the difference between the minimum energy and shoulder is smaller.

For $\varepsilon_r = 1.47$ (near the transition point to the ion–pair form) and for $\varepsilon_r = 1.6$ (close to solid Ar) the energy curve exhibits an almost flat broad minimum for the ion–pair merging into vague shoulder (more visible for $\varepsilon_r = 1.6$) related to the neutral-molecule complex (on the left side). For the field related to $\varepsilon_r = 2.20$ the ionic form (with $R_e(\mathrm{BrH_b}) = 1.836$ Å) is more stable than the neutral-molecule complex related to the shoulder on the left side. The lowest energy curve in Fig. 6 corresponds to $\varepsilon_r = 3.00$, and shows that the ion–pair form (with $R_e(\mathrm{BrH_b}) = 1.926$ Å) has much lower energy than the neutral molecule corresponding to the shoulder (on the left side). These results show that the nature of the hydrogen bond between $\mathrm{BrH_b}$ and NH_3 does indeed depend on the dielectric environment.

The energy curves shown in Fig. 6 clearly differ in shape from those for a harmonic potential. This difference is emphasized in Fig. 7 for $\varepsilon_r = 1.24$ (left) and 1.6 (right). In Fig. 7 the energy is expressed as the difference from equilibrium ($E - E_e$ in $\mathrm{cm^{-1}}$) as a function of the mass-weighted displacement coordinate $q(\mathrm{BrH}) \approx [R(\mathrm{BrH})\text{-}R_e(\mathrm{BrH})] \times (\text{reduced mass})^{1/2}$. These plots show the potential energy function for the proton stretch, on the assumption that the displacement coordinate is indeed pure proton stretch as defined in Sect. 2.2.1.

The shape of the potential energy function for $\nu 2$ has changed from the parabola $2V(q_2) = k(q_2)^2$ to a broader asymmetric curve that is fit better by a one--dimensional quartic function $V(q_2) = a(q_2)^4 + b(q_2)^3 + c(q_2)^2 + d(q_2)$. The solution

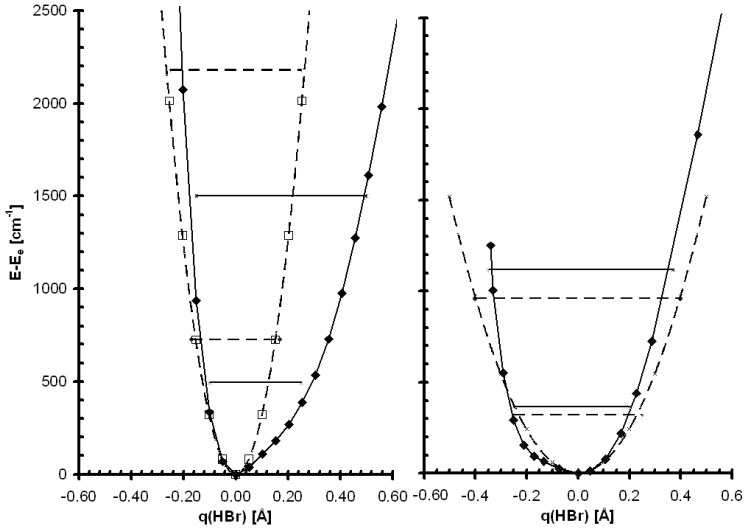

Fig. 7. Comparison of the calculated harmonic (- - -) and anharmonic relaxed potential (filled diamonds and solid line) energy curves for the BrH : NH_3 complex in a dielectric field: left — for $\varepsilon_r = 1.24$; right — for $\varepsilon_r = 1.60$. Horizontal bars show vibrational energy levels $E(v = 0)$ and $E(v = 1)$ for harmonic (- - -) and anharmonic (–) potentials.

[8, 10] of the one-dimensional time-independent Schrödinger equation using this relaxed potential in the Somorjai–Hornig perturbation procedure [14] leads to the value of the anharmonic frequency ν_{anh}(P str) for the transition from the $v = 0$ to the $v = 1$ vibrational level.

In Fig. 7 solid horizontal lines correspond to $v = 0$ and $v = 1$ levels for ν_{anh}(P str) are compared with the corresponding states (dashed horizontal lines) for the harmonic potential. As seen in this figure the difference between the anharmonic and harmonic potentials and energy level spacing is much larger for $\varepsilon_r = 1.24$ (left figure). This contrasts with observation of the right figure ($\varepsilon_r = 1.6$) where the harmonic and anharmonic potentials are very similar, and the corresponding energy levels are quite similar. This comparison implies that the frequency of the proton stretch from the harmonic calculation for $\varepsilon_r = 1.6$ may not be very different from the experimental (anharmonic) frequency in the Ar matrix (ε_r around 1.61–1.63).

Table IV summarizes values of the anharmonic frequencies and $R_0(BrH_b)$ obtained using this procedure for the BrH_b:NH_3 complex in fields with $\varepsilon_r = 1.0$, 1.24, 1.6, 1.8, and 2.2. It is important to notice that the magnitude of the correction for this anharmonicity effect decreases from about 500 cm^{-1} for $\varepsilon_r = 1.00$ to about 100–200 cm^{-1} for $\varepsilon_r = 1.6$–1.8, and then increases again to about 500 cm^{-1} for $\varepsilon_r = 2.2$.

Because the fit of the fourth-order polynomial to the calculated relaxed potential energy curve is not precise, the estimated value of the anharmonic frequency

TABLE IV

Comparison of the calculated harmonic, ν(ha) and anharmonic ν(anh) frequencies and BrH distances at equilibrium R_e(BrH) and R_0(BrH) in the $\nu = 0$ state.

ε_r	ν(ha) [cm^{-1}]	ν(anh) [cm^{-1}]	ν(ha) − ν(anh) [cm^{-1}]	R_e(BrH) [Å]	R_0(BrH) [Å]	$R_e - R_0$ [Å]
1	1665	1127	536	1.511	1.582	–0.071
1.24	1453	1009	444	1.535	1.638	–0.103
1.6	640	750	–110	1.732	1.707	0.025
1.8	929	700	229	1.795	1.758	0.037
2.2	1468	967	521	1.857	1.841	0.016

has an uncertainty on the order of 100 cm^{-1}. The error from the assumption that the normal coordinate q_2 is approximately equal to the mass-weighted internal displacement coordinate might possibly be much larger.

3. Comparison of calculated and experimental spectra

The most complete experimental spectra, including both frequencies and intensities, that are available to us for the isolated BrH : NH_3 complex are those obtained in our laboratory for the complex in solid Ar and in solid N_2 matrices. Infrared spectra were measured with a Nicolet Model 740 FTIR spectrometer sensitive down to 450 cm^{-1}. Solid ammonium bromide (from Aldrich) was sublimed into a stream on matrix gas and the mixture was condensed onto the CsI window mounted on the cold (about 10 K) finger of the cryostat (closed cycle helium cryostat — Displex Model DE-202 from APD Cryogenics, Inc.). Details of the experimental setup and methods of measuring integrated intensities (areas under band contours) as well as those for the analysis of the spectra using Grams, Animol, and Xtrapack programs were described in the earlier papers cited [6–10, 15].

3.1. Spectra in argon matrix

The experimental spectrum of an argon matrix at about 10 K containing BrH and NH_3 is shown in Fig. 8. The top trace shows the spectrum of a dilute matrix with the ratio of Ar : BrH : NH_3 about 1000 : 1 : 1. This spectrum is dominated by the known absorption bands of rotating monomers of NH_3 near 974 cm^{-1}. Other weaker bands of NH_3 monomers are visible near 1638 and 3447 cm^{-1}. The absorption by monomers of BrH is very weak and appears near 2568 cm^{-1}. Other absorption bands appear at 729, 592, and 1147 cm^{-1}. The absorbance of these last three bands increases strongly relative to that of monomers in a spectrum of a matrix with higher concentrations of NH_3 and HBr shown in the middle trace of Fig. 8, indicating that they are related to the BrH_b : NH_3 complex (most likely, one-to-one).

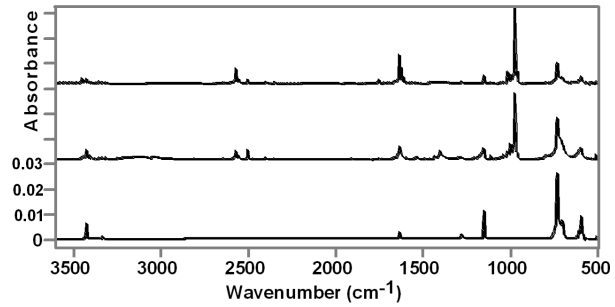

Fig. 8. Experimental infrared spectra of a mixture of BrH and NH_3 in an Ar matrix at about 10 K. Top trace — lower concentration of BrH and NH_3; middle trace — higher concentration of BrH and NH_3. Bottom trace — spectrum of the one to one BrH : NH_3 complex.

Closer examination of the spectra at expanded scales of the top and middle traces in Fig. 8, reveals other weak bands (at 3420, 1630, and 1275 cm^{-1}) that may be related to the 1 : 1 BrH : NH_3 complex. The frequencies of these bands are distinctly different from the well known frequencies of dimers and higher aggregates of NH_3 or of BrH in an Ar matrix (studied and assigned by several authors (e.g. [16, 17, 5] and references therein)).

The spectrum at the bottom of Fig. 8, we believe, is the spectrum of the 1:1 BrH : NH_3 complex in the region from 3500 to 500 cm^{-1}. This spectrum was obtained from the top trace by subtracting the absorption of BrH and NH_3 monomers and that related to traces of their aggregates. The region (1300–500 cm^{-1}) containing the most intense bands is shown in Fig. 9. The relative integrated absorption intensities are given in brackets next to the marked frequencies.

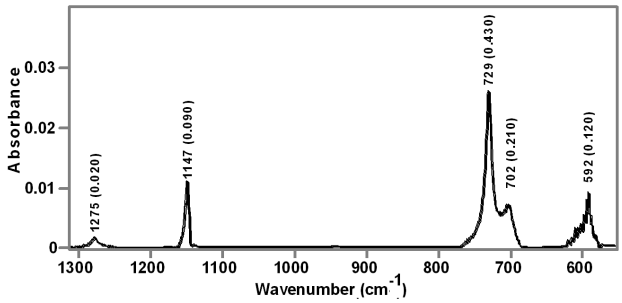

Fig. 9. Region 1300–500 cm^{-1} of the spectrum of the complex (from the bottom trace in Fig. 8) showing the components of the triplet near 700–600 cm^{-1} (with marked frequency and integrated absorbance).

Table V compares the experimental frequencies and absorption intensities with the calculated data from the preceding Sect. 2, for the BrH : NH_3 complex in

TABLE V
Comparison of the calculated frequencies (ν(ha) and ν(anh)) and intensities (A and $A/A(\nu 2)$) for the BrH_b:NH_3 complex in the dielectric field ($\varepsilon_r = 1.6$) with the experimental frequencies (ν_{exp}) and intensities (I_{exp} and I_{exp}/I_Σ) for this complex isolated in an Ar matrix.

Calculation								Experiment		
Norm. mode	ν(ha) [$\frac{1}{cm}$]	ν(anh) [$\frac{1}{cm}$]	A [$\frac{km}{mol}$]	$\frac{A}{A(\nu 2)}$	Sym coor	PED [%]	ID [$\frac{km}{mol}$]	ν_{exp} [$\frac{1}{cm}$]	I_{exp} [$\frac{1}{cm}$]	$\frac{I_{exp}}{I_\Sigma}$
1	2	3	4	5	6	7	8	9	10	11
$\nu 5$	3593	3449[a]	118	0.025	e $NH_{3\,as}$ str	100	104	3444	0.016	0.020
$\nu 1$	3460	3342[b]	22	0.006	a_1 NH_3 sy str	100	20	3345	0.003	0.004
$\nu 6$	1667	1612[c]	63	0.013	e NH_3 as def	95+	86	1630	0.010	0.013
					e NH_3 rock	4+	–28			
$\nu 7$	1314	1271[c]	97	0.02	e BrH_bN be	56+	94	1275	0.02	0.026
					e NH_3 rock	39-	–16			
					e NH_3 as def	5-	20			
$\nu 3$	1291	1153[d]	585	0.125	a_1 NH_3 umb	97-	274	1147	0.09	0.118
					a_1 P str	2-	317			
$\nu 2$	640	750[e]	4713	1	a_1 P str	98-	4811	729	0.430	
								702	0.21	
								592	0.12	
									Σ0.76	1
$\nu 4$	377	362[a]	3	0.0006	a_1 Di str	99+	1	[f]		
$\nu 8$	325	312[a]	18	0.004	e NH_3 rock	60+	4	[f]		
					e BrH_bN be	40+	14			

[a] Scaled by 0.96. [b] Scaled by 0.966. [c] Scaled by 0.967. [d] Scaled by 0.893.
[e] Calculated from the relaxed potential (see previous section). [f] Below studied region.

the dielectric field characterized by $\varepsilon_r = 1.6$ (close to that of solid Ar (1.63 [18] or 1.61 ($= n^2$) [19])). The first eight columns on the left side of the table summarize the calculated data.

The normal modes $\nu 1 - \nu 8$ are listed in column 1. Corresponding calculated harmonic frequencies (unscaled) are listed in column 2. Column 3 presents the related anharmonic frequencies of each mode obtained (with the exception of the proton stretch mode $\nu 2$) by multiplying the harmonic frequency by scaling factors given in the footnotes of Table V. These factors are defined for each normal mode of the complex as equal to the ratio of ν_{exp}/ν_{cal}(ha) for the corresponding mode of NH_3 monomer; ν_{exp} is the experimental frequency observed for NH_3 isolated in Ar matrix and ν_{cal}(ha) is the value calculated at the same level of theory for the monomer at $\varepsilon_r = 1$, listed in the footnotes in Tables II and III. The anharmonic frequency of the proton stretching mode $\nu 2$ is taken from Table IV.

Column 4 shows calculated intensities taken from Tables II and III. Once again we emphasize that the calculated intensity of the proton stretching mode $\nu 2$ is very much larger than that of any other mode. The next most intense mode, $\nu 3$, is 8 times weaker than $\nu 2$. The intensities of the other six fundamental modes are all calculated to be much smaller. In column 5 the ratios of the calculated intensities to that of $\nu 2$ are given for comparison with the experimentally measured relative intensities.

Column 6 lists the internal symmetry coordinates that contribute to each normal mode. The percentage contribution from each to the potential energy distribution (PED; see [8] and references therein) is given in column 7 (signs + or – describe their phase in the vibration). The main contributions from each internal symmetry coordinate to the intensity of the normal mode (the intensity distribution or ID; see [8] and references therein) are given in column 8. It is interesting to note that the main contribution to the PED of $\nu 3$ (97%) comes from the NH_3 umbrella bend symmetry coordinate with only 3% from the proton stretch (P str). However, the ID shows that more than half of the intensity of $\nu 3$ is from the proton stretch internal symmetry coordinate.

Finally we come to the experimental results presented on the right-hand side of Table V. The experimental frequencies for spectra shown in Figs. 8 and 9 are given in column 9 and the corresponding values of integrated absorbance (I_{exp}) are listed in column 10.

Comparison of these experimental results (first for the frequencies in column 10 with the calculated values in column 3) immediately focuses our attention on one of the major discrepancies between the calculated data and the experimental spectrum; namely, there are three strong absorption bands in the experimental spectrum (at 729, 702, and 592 cm^{-1}) and only one strong band in the calculated spectrum at 750 cm^{-1}. Furthermore, there are no other calculated modes nearby.

We believe that the explanation for the appearance of these three strong bands in the experimental spectrum is the Fermi resonance between the very intense fundamental $\nu 2$ and the a_1 components of overtones of lower frequency modes. The low frequency region is inaccessible in our spectrometer, so we cannot measure experimental frequencies below 450 cm^{-1} to examine this hypothesis. Frequencies of overtones can be estimated from the calculated anharmonic frequencies for $\nu 4$ and $\nu 8$ (column 3 of Table V) to give $2 \cdot \nu 4 = 724$ and $2 \cdot \nu 8 = 630$ cm^{-1}. If these estimated values are even close to the true overtone frequencies, it seems very likely that the Fermi resonance involving $\nu 2, 2 \cdot \nu 4$, and $2 \cdot \nu 8$ could be expected to occur to produce a triplet very similar to that observed in the experimental spectrum.

Earlier studies of the spectra of the $BrH : NH_3$ complex [2, 5] have suggested that the band at 592 cm^{-1} might be assigned to the BrH_bN bend ($\nu 7$ in Table V). We do not think that this alternative assignment can be correct for the following reasons. First, the experimental frequency (592 cm^{-1}) is drastically lower than the calculated frequency of this mode (1314 cm^{-1}, see Table V). The difference is much greater than is reasonable to expect for an error due the method of calculation or to some extra anharmonic correction for the BrH_bN bending vibration. Second, the experimental band at 592 cm^{-1} has relatively very high intensity. Its integrated absorbance I_{exp} in column 10 of Table V is only 3.6 times smaller than I_{exp} for the band at 729 cm^{-1}. The calculated intensity for the NH_bBr bend is 48 times lower than the intensity of the $\nu 2$ mode. This discrepancy is much larger than

the experimental error in measuring relative intensities or than the errors in the calculated intensity ratios.

If the triplet at 729, 702, and 592 cm^{-1} is indeed due to the Fermi resonance, then the sum of the intensity from all three bands is expected to be equal to the intensity of the proton stretch. The sum of integrated absorbance for these three components is 0.76. Taking this value as a reference, the relative intensity of each experimental band is obtained and listed in column 11 of Table V. As can be seen in the table these values of experimental relative intensities are very close to the corresponding calculated relative intensities in column 5. Considering the simplicity of the calculation, we are astonished by the quality of this agreement.

3.2. Other matrices and correlations

Because the experimental intensities for BrH : NH_3 in solid Ne and Kr matrices are not given in earlier works [17, 5], experimental results for these matrices shall be discussed very briefly. The recent experimental studies [5] of the BrH : NH_3 complex isolated in solid Ne ($\varepsilon_r = 1.23$ [19]) and solid Kr ($\varepsilon_r = 1.82$ [19]) observe absorption by the hydrogen bonded proton stretching mode ($\nu 2$) at 1080 and 700 cm^{-1}, respectively. Both these frequencies are not far from the anharmonic frequencies given in Sect. 2.3. For dielectric fields with $\varepsilon_r = 1.24$ and $\varepsilon_r = 1.80$, the anharmonic frequencies are 1009 cm^{-1} and 700 cm^{-1}, respectively.

It is well known that N_2 matrix has a larger effect on the infrared spectra of trapped molecules than Ar or Kr matrices [2], despite the fact that ε_r of solid N_2 (1.43 [20]) is smaller than those for solid Ar or Kr. This suggests that the procedure described above for rare gas matrices might not be adequate to account for the effect of an N_2 matrix on the BrH : NH_3 complex. Our exploration of this question is not yet complete, so we shall not say more here about our own experimental studies made for the N_2 matrix, but just say that the very strong band assigned to the proton stretch is observed at 1392 cm^{-1}, in agreement with others [2, 5].

Despite the agreement between calculation and experiment shown in the previous section we are aware that the cavity model is not perfect. However, we do believe that the correlations (between frequencies and distances, for example) based on data in Tables I–III could be valid and useful.

One such correlation between calculated values of $R(BrH_b)$ and proton stretch $\nu 2$ is shown in Fig. 10. An encouraging observation supporting the validity of this correlation is that experimentally known frequencies and R(BrH) distances for HBr monomer [21] and for solid NH_4Br [22, 23] appear to fit the correlation. This last observation inspired us to include experimental frequencies of $\nu 2$ for different matrices on this correlation. These frequencies are marked by the four short horizontal bars crossing the correlation curve. The points where bars cross the correlation provide approximate values for the "experimental" $R(BrH_b)$ for the complex isolated in each matrix. A similar correlation between $\nu 2$ and $R(NH_b)$ can be made.

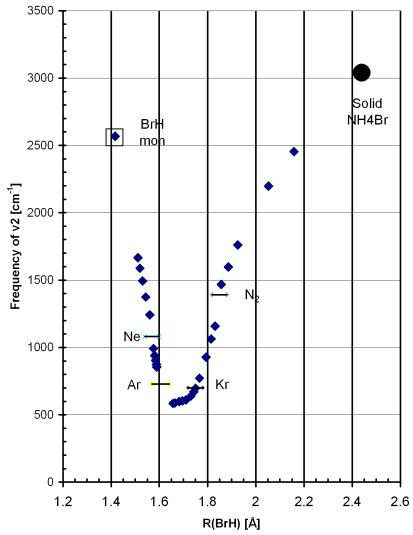

Fig. 10. Correlation between calculated harmonic frequencies of the proton stretching normal mode of the BrH : NH_3 complex with the R(BrH) distance. Points marked by filled diamonds are data from Table I and II; the point marked by □ is for the experimental data for gaseous BrH; point marked by • corresponds to the experimental data for solid ammonium bromide; horizontal bars — mark the experimentally observed frequencies in Ne, Ar, Kr, and N_2 matrices.

We believe that these results suggest that it is possible to carry out reasonably simple calculations that can guide understanding and interpretation of experimental results.

Acknowledgments

We are very grateful to Pierre Chabrier for the development of the Xtrapack program, for measurement of the matrix spectra, and for his stimulating questions about the application of calculations to interpret infrared spectra.

References

[1] J.E. Del Bene, M.J.T. Jordan, P.M.W. Gill, A.D. Buckingham, *Mol. Phys.* **92**, 429 (1997).

[2] A.J. Barnes, Z. Latajka, M. Biczysko, *J. Mol. Struct.* **614**, 11 (2002).

[3] M.J.T. Jordan, J.E. Del Bene, *J. Am. Chem. Soc.* **122**, 2101 (2000).

[4] A. Abkowicz-Bienko, M. Biczysko, Z. Latajka, *Comput. Chem.* **24**, 303 (2000).

[5] L. Andrews, X. Wang, *J. Phys. Chem. A* **105**, 6420 (2001).

[6] K. Szczepaniak, P. Chabrier, W.B. Person, J.E. Del Bene, *J. Mol. Struct.* **436-437**, 367 (1997).

[7] K. Szczepaniak, P. Chabrier, W.B. Person, J.E. Del Bene, *J. Mol. Struct.* **520**, 1 (2000).

[8] K. Szczepaniak, M.M. Szczesniak, W.B. Person, *J. Phys. Chem. A* **104**, 3852 (2000).

[9] W.B. Person, K. Szczepaniak, J.S. Kwiatkowski, *Int. J. Quant. Chem.* **90**, 995 (2002).

[10] K. Szczepaniak, W.B. Person, D. Hadzi, *J. Phys. Chem. A* **109**, 6710 (2005).

[11] Gaussian 98, Revision A.9, M.J. Frisch, G.W. Trucks, H.B. Schlegel, G.E. Scuseria, M.A. Robb, J.R. Cheeseman, V.G. Zakrzewski, J.A. Montgomery, Jr., R.E. Stratmann, J.C. Burant, S. Dapprich, J.M. Millam, A.D. Daniels, K.N. Kudin, M.C. Strain, O. Farkas, J. Tomasi, V. Barone, M. Cossi, R. Cammi, B. Mennucci, C. Pomelli, C. Adamo, S. Clifford, J. Ochterski, G.A. Petersson, P.Y. Ayala, Q. Cui, K. Morokuma, D.K. Malick, A.D. Rabuck, K. Raghavachari, J.B. Foresman, J. Cioslowski, J.V. Ortiz, A.G. Baboul, B.B. Stefanov, G. Liu, A. Liashenko, P. Piskorz, I. Komaromi, R. Gomperts, R.L. Martin, D.J. Fox, T. Keith, M.A. Al-Laham, C.Y. Peng, A. Nanayakkara, M. Challacombe, P.M.W. Gill, B. Johnson, W. Chen, M.W. Wong, J.L. Andres, C. Gonzalez, M. Head-Gordon, E.S. Replogle, J.A. Pople, Gaussian, Inc., Pittsburgh PA, 1998.

[12] I. Mills, T. Cvitas, K. Homann, N. Kallay, K. Kuchitsu, *Quantities, Units and Symbols in Physical Chemistry*, 2nd ed., International Union of Pure and Applied Chemistry, Blackwell Science, Oxford 1993.

[13] A.E. Frisch, M.J. Frisch, *Gaussian 98, User's Reference*, 2nd ed., Gaussian Inc., Pittsburgh, PA 1999.

[14] R.I. Somorjai, D.F. Hornig, *J. Chem. Phys.* **36**, 1980 (1962).

[15] P. Chabrier, Ph.D. Thesis, University of Florida, 1998.

[16] L. Abouaf-Marguin, M.E. Jacox, D.E. Milligan, *J. Mol. Spectrosc.* **67**, 34 (1977).

[17] A.J. Barnes, M.P. Wright, *J. Chem. Soc., Faraday Trans. 2* **82**, 153 (1986).

[18] H.E. Hallam, G.F. Scrimshaw, in: *Vibrational Spectroscopy of Trapped Species*, Ed. H.E. Hallam, Wiley, New York 1973, p. 45.

[19] D.M. Kolb, F. Forstmann, in: *Matrix Isolation Spectroscopy*, Eds. A.J. Barnes, W.J. Orville-Thomas, A. Muller, R. Gaufres, NATO ASI Series C, Vol. 76, D. Reidel, Dordrecht, The Netherlands 1981, p. 350.

[20] S. Pilla, J.A. Hameda, K.A. Muttalib, N.S. Sullivan, *Phys. Lett. A* **256**, 75 (1999).

[21] G. Herzberg, *Molecular Spectra and Molecular Structure I. Diatomic Molecules*, 2nd ed., Van Nostrand, New York 1950, p. 534.

[22] E.L. Wagner, D.F. Hornig, *J. Chem. Phys.* **18**, 305 (1950).

[23] W.C. Hamilton, J.A. Ibers, *Hydrogen Bonding in Solids*, W.A. Benjamin, Inc., New York 1961, p. 224-6.